JOURNAL OF SPACECRAFT AND ROCKETS
Vol. 47, No. 1, January–February 2010

X-43A Flush Airdata Sensing System Flight-Test Results

Ethan Baumann,* Joseph W. Pahle,† and Mark C. Davis‡
NASA Dryden Flight Research Center, Edwards, California 93523
and
John Terry White§
Tybrin Corporation, Edwards, California 93523

DOI: 10.2514/1.41163

NASA has flight tested a flush airdata sensing system on the Hyper-X research vehicle (X-43A) at hypersonic speeds during the course of two successful flights. The flush airdata sensing system was calibrated to operate between Mach 3 and Mach 8, and flight-test data were collected between Mach 1 and Mach 10. The flush airdata sensing system acquired pressure data from surface-mounted ports and generated a real-time angle-of-attack estimate onboard the X-43A. The collected data were primarily intended to evaluate the flush airdata sensing system performance, and the estimated angle of attack was used by the flight control algorithms on the X-43A for only a portion of the first successful flight. A separate set of algorithm calibrations based on wind-tunnel data was found to match the flight results better than the analytically derived calibrations at the lower Mach numbers. This paper provides an overview of the flush airdata sensing system and angle-of-attack estimation algorithms, the in-flight angle-of-attack estimation algorithm performance, and the comparisons between flight-test data, analytical predictions, and wind-tunnel results. Flight-test results indicate that the flush airdata sensing system is a viable technique for generating a real-time angle-of-attack estimate at hypersonic velocities.

Nomenclature

C_{P24}	=	ports 2 and 4 differential pressure coefficient
C_{P25}	=	ports 2 and 5 differential pressure coefficient
C_{P35}	=	ports 3 and 5 differential pressure coefficient
P_2	=	port 2 pressure reading, psf
P_3	=	port 3 pressure reading, psf
P_4	=	port 4 pressure reading, psf
P_5	=	port 5 pressure reading, psf
$\bar{q}$	=	dynamic pressure, psf
α	=	angle of attack, deg
β	=	angle of sideslip, deg

I. Introduction

A FLUSH airdata sensing (FADS) system [1] was flight tested on the Hyper-X research vehicle (X-43A), a free-flying, airframe-integrated supersonic combustion ramjet (scramjet) vehicle. The X-43A vehicles were successfully flown twice and demonstrated scramjet operation at nearly Mach 7 and nearly Mach 10. Real-time estimates of angle of attack (α) were generated by the onboard FADS α estimation algorithm. Data were collected during these two flights to allow for a postflight analysis of the FADS α estimation algorithm's performance.

Scramjet performance is highly sensitive to α, and an accurate, real-time method of estimating α can ensure optimal scramjet performance. Estimating α solely from the inertial navigation system (INS) is difficult because of atmospheric variations, winds, and sensor installation and performance. Initially, strict requirements to measure and control α for optimal scramjet operation led to the development of a research FADS system for the X-43A to explore the concept. The α measurement and control requirement varied for the different mission phases, but the general requirement was to measure and control the vehicle α within an absolute accuracy of 0.5 deg. Before the flights, the real-time α estimation algorithms were not deemed mature enough to replace or supplement the inertial α measurement during the scramjet engine tests. However, the algorithms were active during both flights and used to correct the inertial α measurement during the postengine test portion of the X-43A Mach 7 mission. The scramjet engines tested on the X-43A flight vehicles were designed with operating margin at the engine test points, which resulted in the accuracy of the INS α estimate being deemed acceptable during the short duration test points.

The FADS data collected during the ascent and postengine test portions of the Mach 7 and Mach 10 missions are presented. The performance of the real-time α estimation algorithms using an analytically derived calibration and one derived from wind-tunnel data is also presented. The FADS α estimate calculated with the real-time algorithm matches the postflight reconstructed α from the best estimated trajectory data within 1 deg, and usually much better for both the Mach 7 and Mach 10 missions.

II. Project Description

The goal of the NASA Hyper-X program was to demonstrate an advanced, airframe-integrated, airbreathing, hypersonic propulsion system in flight, thus validating the supporting design tools and technologies [2,3]. The program sought to design, build, and flight test a series of three small, autonomous, scramjet-powered X-43A vehicles at Mach 7 and Mach 10. Two of the vehicles were intended for missions at Mach 7 and one vehicle was intended for a mission at Mach 10. The first flight was intended to reach Mach 7 and was attempted on 2 June 2001. The Hyper-X launch vehicle (HXLV), used to boost the X-43A to the test condition, lost control shortly after launch resulting in the loss of both the HXLV and X-43A [4]. During the second flight, hereafter referred to as the Mach 7 mission and flown on 27 March 2004, the X-43A successfully demonstrated the in-flight operation of the scramjet [5]. All of the goals for that mission were achieved, including positive acceleration of the vehicle by the scramjet. The third and final flight, hereafter referred to as the

Presented as Paper 6570 at the AIAA Atmospheric Flight Mechanics Conference and Exhibit, Honolulu, HA, 18–21 August 2008; received 22 September 2008; revision received 8 October 2009; accepted for publication 21 October 2009.

*Aerospace Engineer, Controls and Dynamics Branch, Post Office Box 273/Mail Stop 4840D.
†Aerospace Engineer, Controls and Dynamics Branch, Post Office Box 273/Mail Stop 4840D. Senior Member AIAA.
‡Aerospace Engineer, Aerodynamics and Propulsion Branch, Post Office Box 273/Mail Stop 4840D. Member AIAA.
§Aerospace Engineer, Post Office Box 273/Mail Stop 4840D. Senior Member AIAA.

Mach 10 mission, was flown on 16 November 2004, and all of the goals for this mission were also accomplished [6]. During both successful missions, the X-43A was in controlled autonomous flight from the point of separation from the HXLV to impact in the Pacific Ocean [7,8].

III. X-43A Vehicle Description

As shown in Fig. 1, the X-43A was a sharp-nosed unmanned autonomous vehicle that measured approximately 12 ft long and 5 ft wide, and weighed approximately 3000 lb. All three vehicles had the same outer mold line; the primary difference among the vehicles was the internal engine flowpaths. The scramjet engine was attached to the underside of the X-43A and contained a cowl door on the leading edge of the engine. The cowl door allowed air to flow through the engine only during the scramjet test, and was otherwise closed. The X-43A had four control surface effectors, a left and right all-moving wing used to control the pitch and roll axes, and twin rudders used to control the yaw axis. The nose and wing leading edges were carbon–carbon composites [9].

IV. X-43A Vehicle Mission Description

The X-43A mission profiles were similar for the Mach 7 and Mach 10 missions. The principal difference between the two flights was the higher Mach number attained during the Mach 10 mission, which resulted in a correspondingly longer descent trajectory. Figure 2 shows an overview of the X-43A mission. The launch, scramjet experiment, and descent portions of the mission were conducted off the coast of southern California. The entire configuration, known as the X-43A stack, was carried under the wing of the NASA Dryden Flight Research Center (DFRC) NB-52B (The Boeing Company, Chicago, Illinois), ship number 008. The X-43A was boosted to the test condition by the HXLV, a modified Pegasus® rocket (Orbital Sciences Corporation, Dulles, Virginia). The X-43A separated at Mach 7.075 at an altitude of 93,932 ft during the Mach 7 mission [5], and at Mach 9.702 at an altitude of 109,653 ft during the Mach 10 mission [10]. Several seconds after separation the cowl door was opened, the vehicle was stabilized at the desired test condition, and the scramjet engine test was conducted. The scramjet experiment phase lasted approximately 45 s for the Mach 7 mission and 30 s for the Mach 10 mission. Following the primary mission, the cowl door

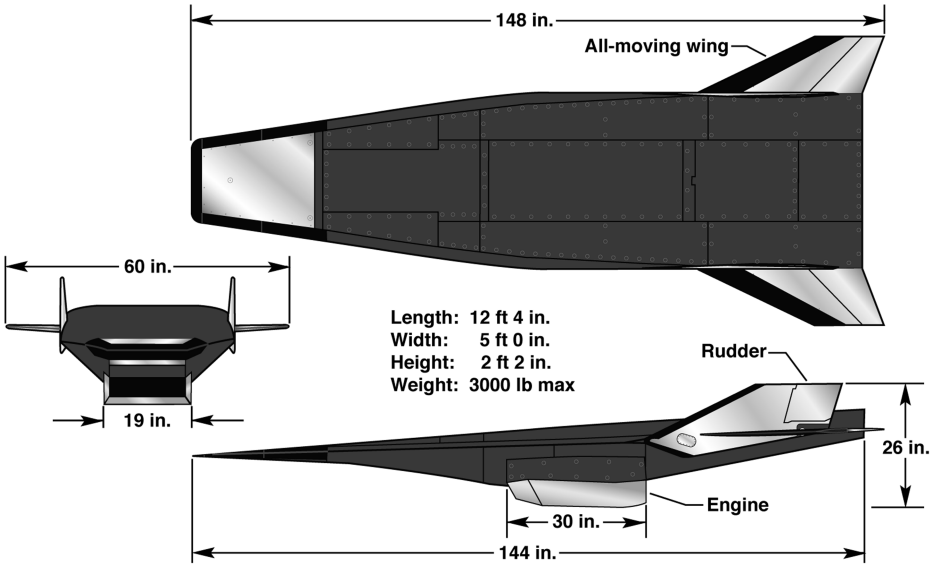

Fig. 1 X-43A vehicle three-view.

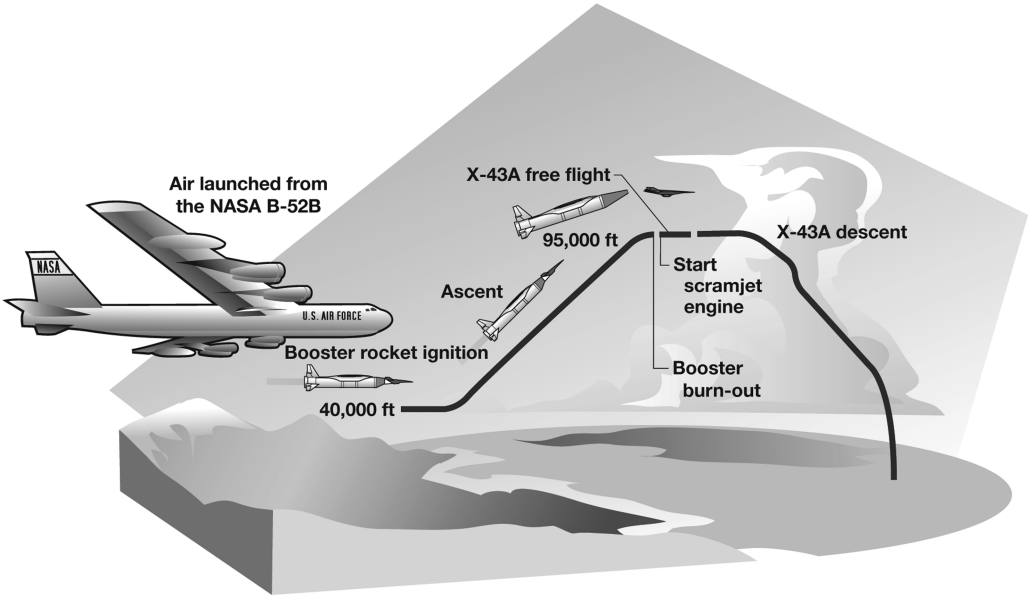

Fig. 2 X-43A flight trajectory.

was closed and an unpowered trajectory was flown to impact into the Pacific Ocean. During the descent portion of the two missions, a series of parameter identification (PID) maneuvers were performed at every integer Mach number down to Mach 2 [11,12]. These maneuvers began at Mach 5 during the Mach 7 mission and at Mach 8 during the Mach 10 mission. The Mach 7 mission PID maneuvers consisted of a series of step inputs, frequency sweeps, and an α sweep. The Mach 10 mission PID maneuvers consisted of two sets of frequency sweeps. The flight data shown in this paper are from the boosted ascent and unpowered postexperiment descent portions of these flights with the cowl door closed.

V. Flush Airdata Sensing System Architecture Overview

The pressure port layout for the FADS system is discussed in detail in [1]. The architecture details are summarized in this section. The scope of this paper is limited to the α estimation capability of the FADS system; therefore, only the architecture elements specific to the α estimate calculation are discussed. The complete FADS system consists of a matrix of nine pressure ports, of which only four are used to estimate α. Figure 3 shows the locations of the four ports along the centerline of the upper and lower surface (ports 2–5), which were used to indirectly estimate the α in real time. The pressure ports on the upper and lower ramp surfaces had a diameter of 0.04 in. and were drilled normal to the surface.

The port pressures were sensed using a combination of absolute and differential precision pressure transducers (PPT). Tubing connected the pressure ports to the PPTs. All of the PPTs had serial digital outputs, which were connected through an individually addressable, multidrop RS-485 bus. Figure 4 shows the layout of these sensors. Differences between the pairs of upper and lower ramp surface pressures (ports 2 and 4, ports 3 and 5) were sensed by differential pressure transducers to provide a high-accuracy and high-resolution measurement for use by the real-time α algorithm. Ports 2 and 5 were also teed to an absolute pressure transducer that allowed the absolute pressure level at these ports to be sensed. This combination of absolute and differential ports allowed for a calculation or measurement of the absolute pressure at each port while retaining the high accuracy differential measurements for the α algorithm. Figure 5 shows the underside of the X-43A forebody, and indicates the locations of ports 4 and 5, and the boundary layer trip strip location between the two ports [1]. The boundary layer trip strip was placed at this position to ensure turbulent airflow entered the scramjet engine. The port locations, PPT configuration, and boundary-layer trip location were the same for the Mach 7 and Mach 10 missions. Table 1 lists the PPTs, associated pressure ports, sensor range and accuracy, and flights for which the data are available.

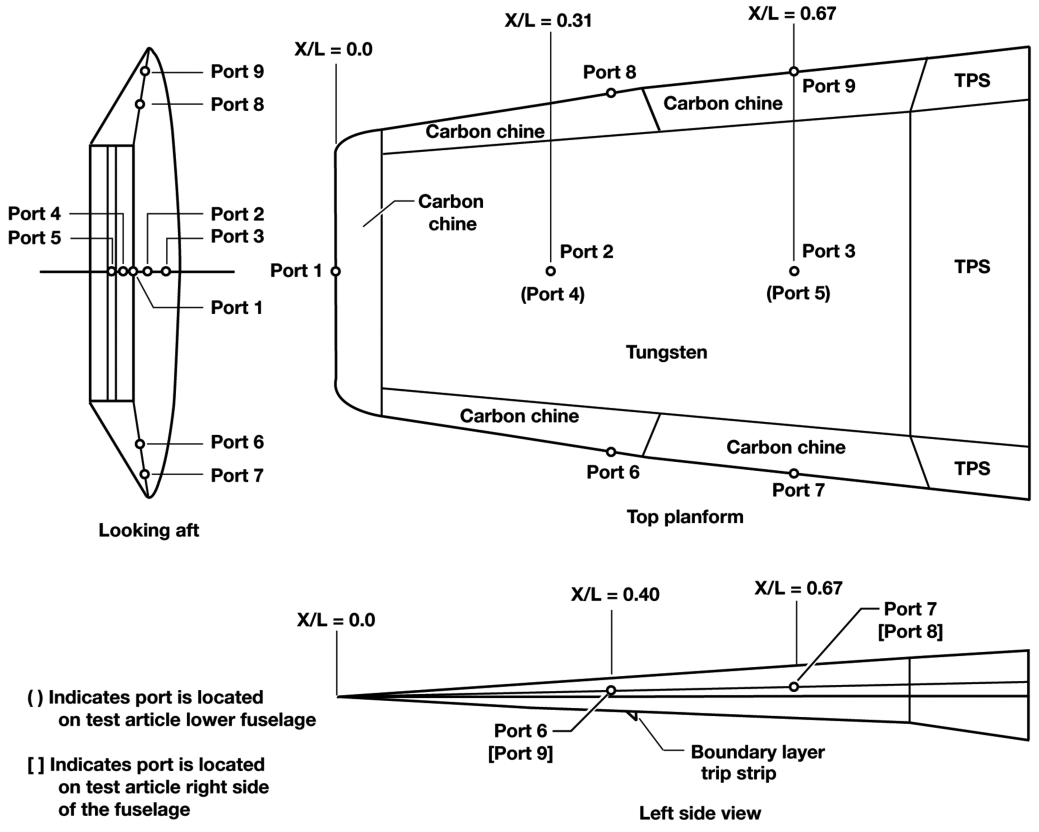

Fig. 3 FADS system port layout.

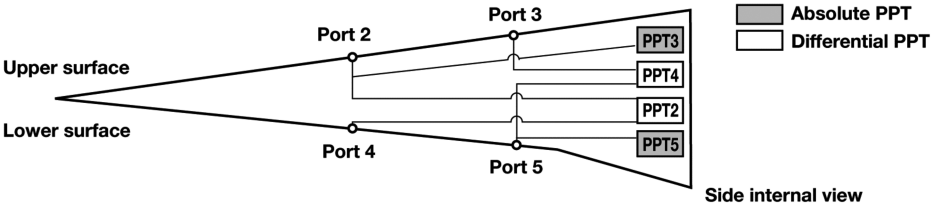

Fig. 4 FADS system port and PPT layout for the Mach 7 and Mach 10 missions.

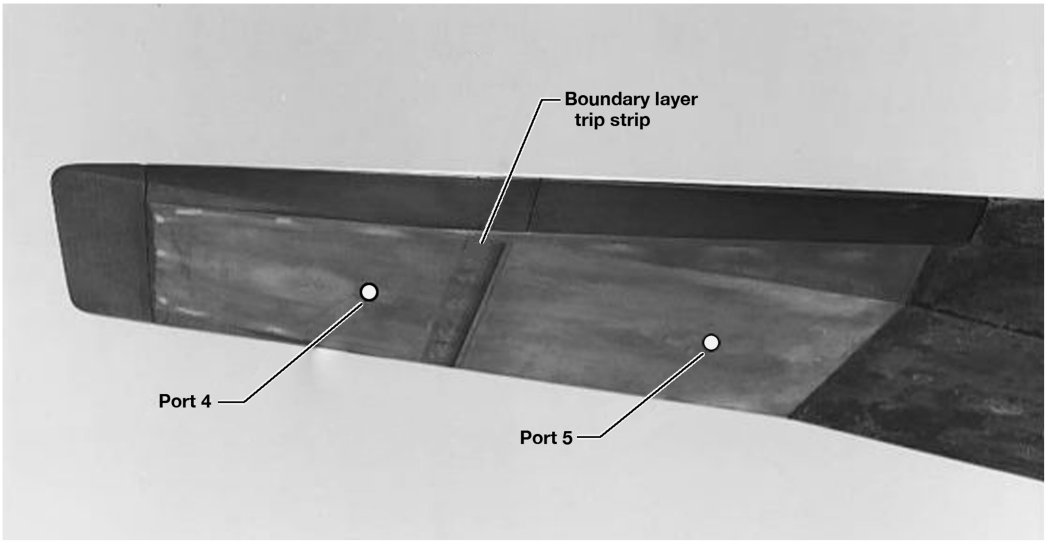

Fig. 5 X-43A lower surface showing the locations of ports 4 and 5 and the boundary layer trip strip.

VI. Flush Airdata Sensing System Angle-of-Attack Estimation Algorithm

Pressure port data were collected continuously throughout the two missions, including the captive carry, ascent, engine experiment, and descent phases. Real-time algorithms were developed for the α estimation calculation. These algorithms were intended for use between Mach 3 and Mach 8, because wind-tunnel data were available to validate the algorithm only in this Mach number range.

The primary function of the real-time α estimation algorithm was to provide a pneumatically based measurement estimate of the bias in the INS-derived α. The FADS α estimate blended with the inertial α estimate to provide an air-mass-corrected value for use by the flight control laws. The FADS α estimate is used to estimate the low-frequency portion of an air-mass corrected α, whereas the INS provides the high-frequency component through an inertial velocity based calculation. At high velocities, the wind component of α is relatively small compared with the total vehicle velocity. As a result, the INS α is a good estimate of the air-mass relative α. As the velocity decreases, the wind component increases, and the INS estimate is less accurate.

Because the algorithm was designed for use as an input to the flight control laws during the free-flight portion of the X-43A mission, a number of error checks and additional safeguards were added to the algorithm. The FADS α estimation algorithm was executed in real time throughout both the Mach 7 and Mach 10 missions, but was only used to aid the inertial solution during the period following the scramjet engine experiment of the Mach 7 mission. The reason for this decision is that the FADS α estimation algorithm was not considered mature enough for use during the scramjet engine experiment. The FADS α estimation algorithms were not used to aid the inertial α estimate during the Mach 10 mission, because sufficient time was not available between the two missions to validate the algorithm for operation above Mach 8, analyze Mach 7 mission data, develop updates derived from the Mach 7 mission analysis, and implement changes to the flight software.

The FADS α estimation algorithms are discussed in detail in [1] and summarized here. The PPT measurements used by the real-time algorithm were updated at 25 Hz, and the algorithm was executed at 100 Hz as part of the flight control software. The FADS α estimate was derived from three independent α estimates, hereafter referred to as "FADS1," "FADS2," and "FADS3," The FADS1 estimate was derived from the differential pressure measurement between ports 2 and 4. The FADS2 estimate was derived from the differential pressure measurement between ports 3 and 5. The final α estimate, FADS3, was derived from the difference between the absolute pressure measurements from ports 2 and 5.

Table 1 Flush airdata sensing system pressure ports

Sensor	Port(s)	Sensor type	Range, lbf/ft^2 Min	Range, lbf/ft^2 Max	Accuracy, lbf/ft^2
PPT 2	2, 4	Differential	−720	720	0.18
PPT 3	2	Absolute	0	2160	0.54
PPT 4	3, 5	Differential	−720	720	0.18
PPT 5	5	Absolute	0	2160	0.54

The FADS α estimates were calculated as shown in Eq. (1). The differential pressure coefficients C_{P24}, C_{P35}, and C_{P25} were scheduled as a function of Mach number and calculated from the FADS pressure port database (DB), which consisted of pressure values for each port as a function of Mach number and α [1]. The Mach number and dynamic pressure used in the FADS algorithm and coefficient table lookup was calculated onboard using inertial velocity from the vehicle's INS along with a representative atmospheric model. At hypersonic velocities, the inertially derived Mach number and dynamic pressure are sufficiently accurate to be used in the FADS algorithm, because winds are a relatively small contributor to the vehicle's velocity. In addition, the onboard atmospheric model used to calculate Mach and dynamic pressure is considered representative of the day of flight atmosphere

$$\text{FADS 1} = \left(\frac{P_2 - P_4}{\bar{q}}\right) C_{P24} \tag{1a}$$

$$\text{FADS 2} = \left(\frac{P_3 - P_5}{\bar{q}}\right) C_{P35} \tag{1b}$$

$$\text{FADS 3} = \left(\frac{P_2 - P_5}{\bar{q}}\right) C_{P25} \tag{1c}$$

Pressure lags exist in any pneumatically based system, and these lags are accounted for in the FADS algorithm. Pneumatic lag models were developed for each PPT measurement and used in the FADS algorithm to determine out-of-range or failed sensors. It was necessary to develop a separate lag model for each PPT, because the amount of tubing between the pressure ports and PPTs varied. The pressure lag between the pressure ports and the PPTs was modeled as a first order lag. From wind-tunnel tests, it was observed that the lag characteristic for the differential pressure measurements remains relatively constant across the pressure range. As a result of this observation, the lag models for a differential pressure measurement are only a function of Mach and not a function of input pressure. The

lag constants for each PPT were developed with an analog matching technique, which used the wind-tunnel test data. Further information on the development of the FADS algorithm's pneumatic lag model is included in [1].

Figure 6 shows how the three individual FADS α estimates were combined with the inertial α measurement to generate the FADS α estimate for use by the flight control laws. The inertial α was passed through a Mach number-dependant pneumatic lag model for each of the FADS α estimates. Inertial Mach was used to schedule the lag models. The lagged α values were subtracted from each of the three FADS α estimates, and these differences were evaluated to check the validity of the estimates. A FADS α estimate was considered valid if it was within a predetermined tolerance of the lagged inertial α. The differences between the three FADS α estimates and the lagged inertial value were averaged over the valid FADS α estimates. This average was passed through a low-pass filter resulting in a low-frequency bias term, hereafter referred to as the FADS bias, and was added to the inertial α. The final result was the FADS α estimate, which had a low-frequency component corrected by the FADS α algorithms, and a high-frequency component from the inertial α. If all three FADS α estimates were invalid, the value input to the low-pass filter was set to zero, resulting in no correction to the inertial α.

A FADS pressure database based on viscid and inviscid methods was used to develop the differential pressure coefficients used in the FADS α estimation algorithm. Viscid and inviscid methods were used to calculate the pressure values analytically for the upper and lower surfaces of the X-43A forebody surface ramps. The inviscid calculations use the oblique shock relations [13] to model compressions and expansions were analyzed using the Prandtl–Meyer equations [13]. Viscous interaction-induced pressures were estimated using the statistical correlations for flat plates in laminar flow [14,15]. The FADS pressure database was developed for the Mach 2–Mach 8 flight range. Above Mach 8, the database was linearly extrapolated to generate pressure port predictions. The viscid and inviscid theory predictions were considered most applicable at Mach 3 and above. The analytical calculations do not account for the presence of the boundary-layer trip strip between the two lower pressure ports. The FADS pressure database derived from these pressure predictions is hereafter referred to as the analytically derived database.

Wind-tunnel data were collected [16] and compared with the analytically derived FADS pressure database. In general, wind-tunnel data compared well with analytical predictions except for differences in the lower aft pressure port readings at the lower Mach numbers. Wind-tunnel data were collected during constant α and pitch-pause runs with sweeps in angles of attack at the following Mach numbers: 2, 2.25, 2.5, 2.75, 3, 4, 5, 6, and 8. Data were obtained over an α range of -6–12 deg. In the pitch-pause maneuvers, data were obtained in 1 deg increments. The dwell time at each pitch-pause data point was approximately 15 s [1]. Problems with the wind-tunnel test hardware and data measurement system resulted in the data collected below Mach 3 being suspect. In addition, the wind-tunnel data showed an unanticipated decrease in the pressure at the lower aft FADS port (port 5) below Mach 5 as compared with the analytically derived database. This pressure difference between the wind-tunnel data and analytical predictions increases with decreasing Mach number. The boundary-layer trip strip located between ports 4 and 5 was examined and eliminated as a cause for the decreased wind-tunnel test pressure port reading. Wind-tunnel tests, conducted as part of the FADS system development, were performed with boundary-layer trip strips of varying sizes and compared with tests conducted without the boundary-layer trip strips [16]. No significant differences were observed in the port 5 pressure port readings between the wind-tunnel tests conducted with and without a boundary-layer trip strip. The reason for the decreased lower aft pressure port reading, as compared with theory, is not understood.

Because of the differences in the analytically derived database and the wind-tunnel test results, a second database was developed from the wind-tunnel data. The FADS pressure port database generated from the wind-tunnel data is hereafter referred to as the wind-tunnel derived database. Only one wind-tunnel run at each Mach number was used to generate the wind-tunnel derived database. The raw wind-tunnel data were corrected with biases based on two criteria. The differential PPT data from the wind-tunnel test should read zero at a specific α determined from the forebody geometry. Additionally, the ratio of the absolute PPT reading and total pressure should be equal to one when the forebody is at an α equal to the ramp angle of the upper or lower surface. These biases were then applied to the wind-tunnel data to generate the wind-tunnel derived database. The magnitude of the biases is relatively small, generally between 0.1 to 2.0 psf, and some of the biases are within the PPT measurement accuracy of 0.18 psf for the differential measurements and 0.54 psf for the absolute measurements.

Figure 7 displays the pressure port comparisons between the analytically derived database, the raw wind-tunnel data, and the wind-tunnel derived database at Mach 8. Good agreement exists between the analytically derived and the wind-tunnel derived databases at Mach 8. The same pressure port comparisons at Mach 3 are shown in Fig. 8. At Mach 3, the two databases predict similar pressures for the forward ports, and differences are observed in the aft ports. For the aft ports, the wind-tunnel derived database predicts lower pressures than the analytically derived database as α increases, and slightly higher pressures at negative α. The greatest differences between the analytically derived and wind-tunnel derived databases for port 3 are on the order of 10 psf. The port 5 pressures from the wind-tunnel derived and analytically derived databases are as much as 50 psf different at the highest α.

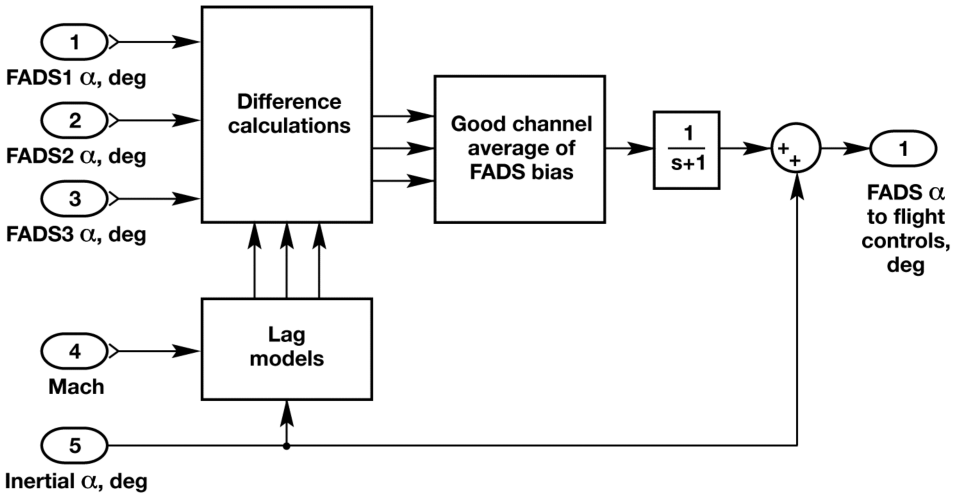

Fig. 6 Complementary filter implementation.

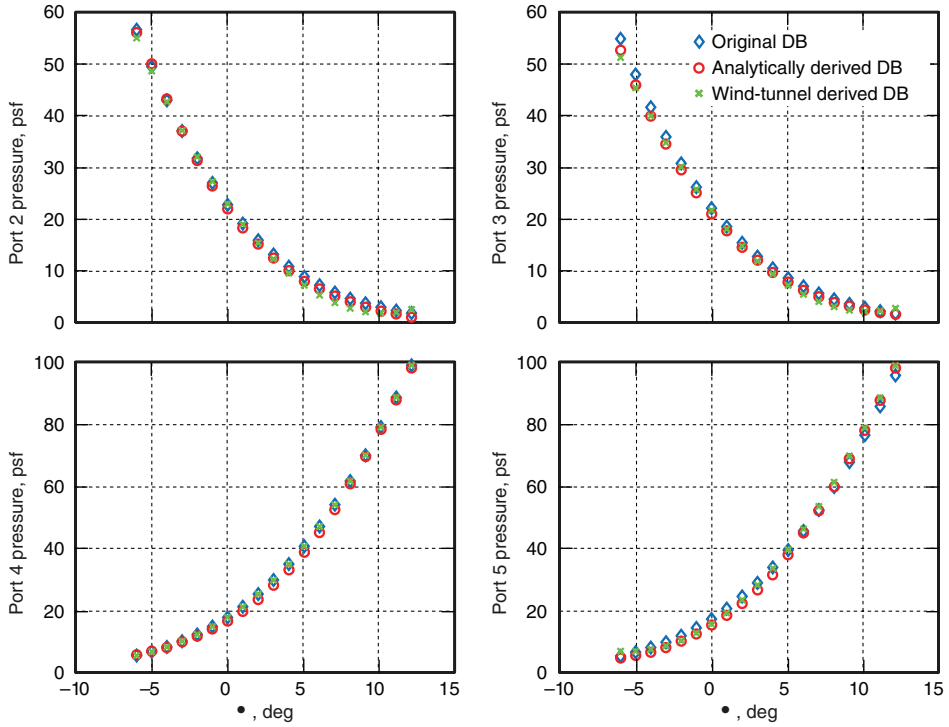

Fig. 7 Mach 8 pressure port predictions.

VII. Best Estimated Trajectory

A best estimated trajectory (BET) was developed for both the Mach 7 mission [17] and the Mach 10 mission [10]. The BET was generated from in-flight telemetry data, which was combined with various redundant measurements, to generate maximum-likelihood estimates of the vehicle position, velocity, and orientation time histories along with estimates of their uncertainties. These results were then combined with an independent atmosphere reconstruction, which included uncertainties, to yield wind-relative parameters that are required for detailed analysis of the vehicle performance during flight conditions. The independent atmosphere reconstruction used balloon data from various locations on and around the Pacific Ocean test range. Atmospheric and wind data along the actual flight path of the X-43A were not available, so the BET data has increasing

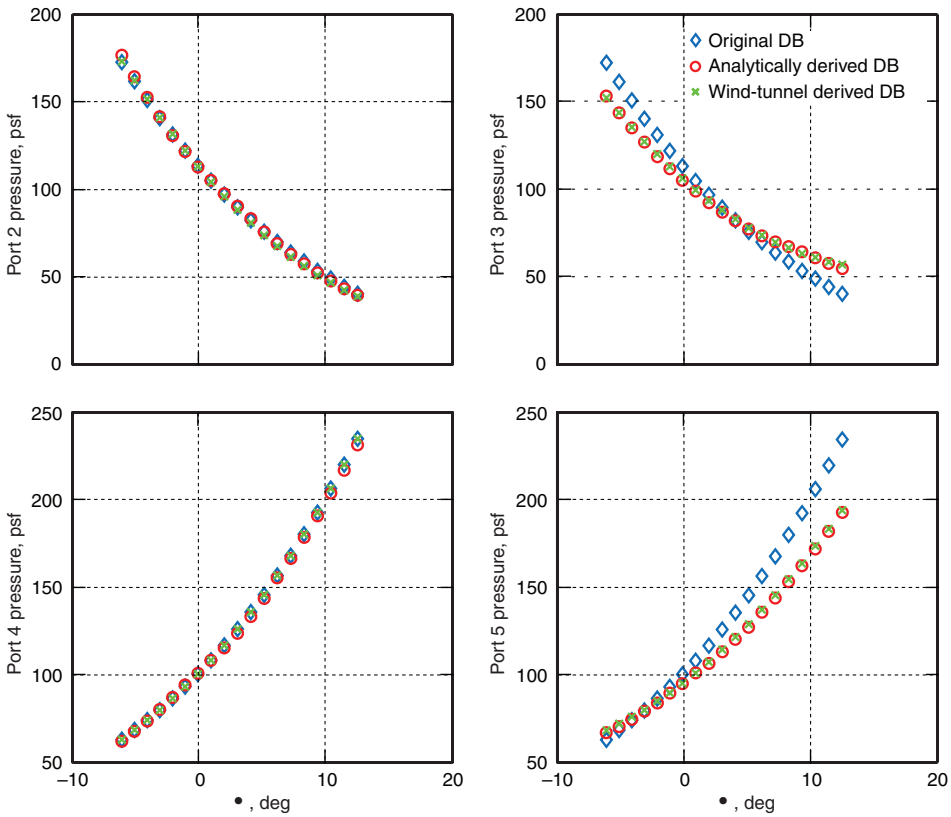

Fig. 8 Mach 3 pressure port predictions.

uncertainty as the missions progress. The BET data referred to in this paper are provided from the BET reconstruction efforts.

VIII. Mach 7 Mission and Mach 10 Mission Comparisons

Figure 9 shows the BET α during the ascent and descent portions of the two missions as a function of the BET. All figures displaying data from the ascent portion of the missions are plotted against increasing Mach number, which is consistent with plotting as a function of increasing time. Correspondingly, the data from the descent portion of the mission are plotted against decreasing Mach number. Figure 10 shows the BET $\bar{q}$ during the ascent and descent portions of the two missions. As shown in Figs. 7 and 8, the X-43A flew at different α and $\bar{q}$ profiles during the two flights. As a result, direct comparisons of FADS data between the two missions are not possible.

IX. Flush Airdata Sensing Pressure Port Comparisons

Figure 11 shows the forward pressure ports (ports 2 and 4) readings during the ascent portion of the Mach 7 mission. The flight data are compared with the analytically derived and wind-tunnel derived database predictions. Flight data from the BET were used to generate the pressure predictions with the two databases. The wind-tunnel derived and analytically derived databases track the flight data similarly for the forward port measurements. The port 2 predictions are within 15 psf of the flight values with the greatest difference occurring around Mach 7. The port 4 predictions are within 7 psf of the flight values.

The aft pressure port readings from the ascent portion of the Mach 7 mission are compared with the wind-tunnel derived and analytically derived database predictions as shown in Fig. 12. The wind-tunnel derived database matches the flight pressure readings significantly better at the lower Mach numbers. The prediction from the wind-tunnel derived database is within 10 psf of the flight data for port 3 and within 5 psf of the flight data for port 5.

Figure 13 shows the forward pressure port readings from the descent portion of the Mach 7 mission compared with the wind-tunnel derived and analytically derived databases. Both databases exhibit the same trends as the flight data, but are biased from the flight readings. The wind-tunnel derived database tracks the flight readings for port 2 to within 3 psf, which is slightly better than the analytically derived database. Predictions from the wind-tunnel derived and analytically derived databases indicate a bias of approximately 15 psf from the flight readings for port 4. The cause for the bias between the flight data and the two databases is not known, but is possibly due to a bias in the flight PPT.

Figure 14 shows the aft pressure port comparisons during the descent portion of the Mach 7 mission. The wind-tunnel derived database predictions are generally within 2 psf of the port 3 flight readings and biased 5 psf high when compared with the port 4 flight data. The analytically derived database exhibits an increasing pressure difference for port 5 as the Mach number decreases. The wind-tunnel derived database also provided better matching of the port 3 flight data below Mach 5.

The Mach 10 mission pressure comparisons are similar to those of the Mach 7 mission. Figure 15 shows the aft pressure port comparisons for the descent portion of the Mach 10 mission. The wind-tunnel derived database predictions for port 3 compare slightly better than those of the analytically derived database above Mach 5. Similar to the Mach 7 mission comparisons, the wind-tunnel derived database predictions for port 5 match the flight pressure readings of the Mach 10 mission significantly better than the analytically derived database as Mach number decreases.

A constant bias is often seen between the flight data and the analytical and wind-tunnel derived databases. The cause for this bias

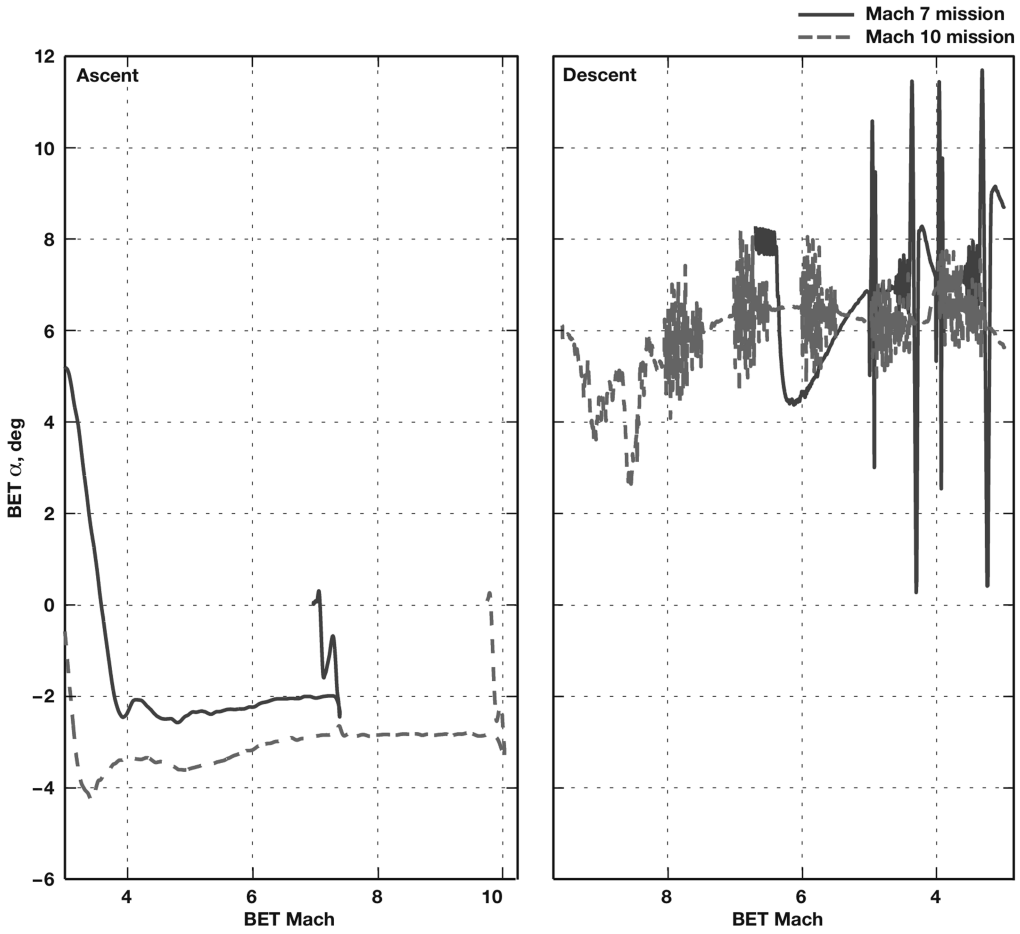

Fig. 9 BET α comparison between the Mach 7 and Mach 10 missions.

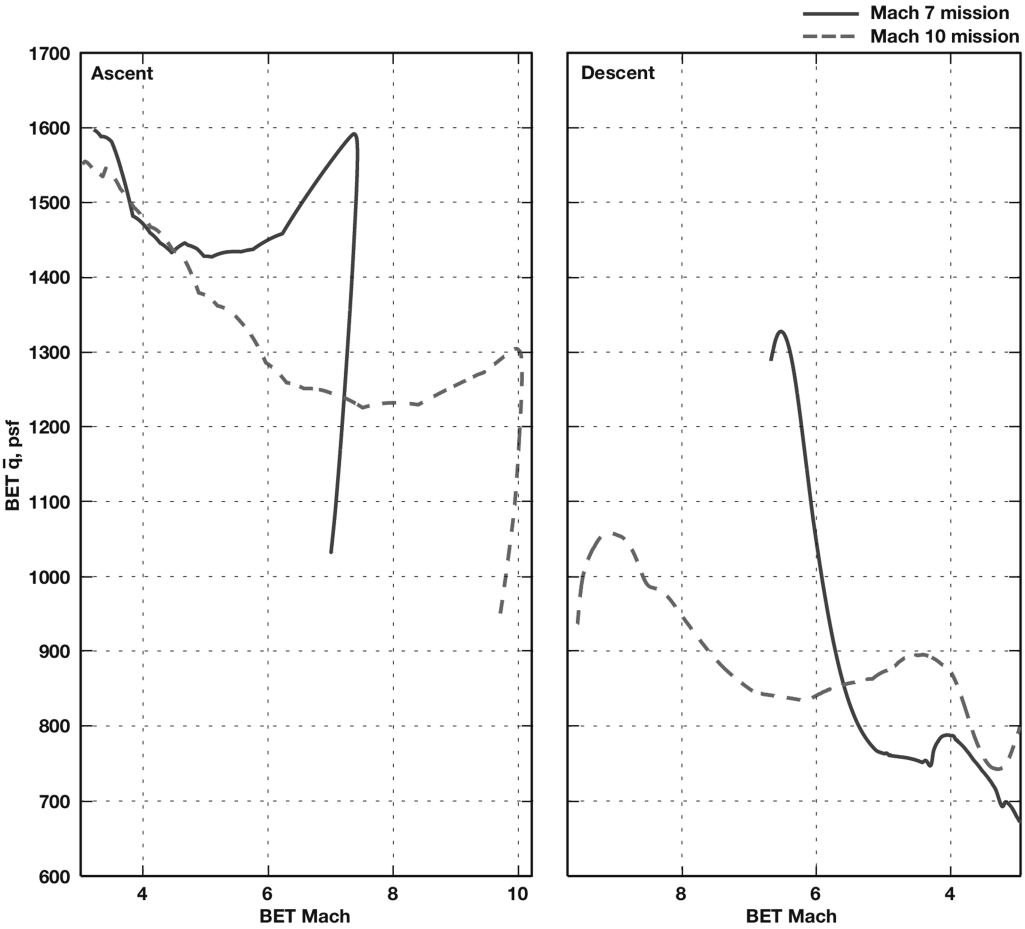

Fig. 10 BET $\bar{q}$ comparison between the Mach 7 and Mach 10 missions.

is currently unknown, but is possibly due to a calibration issue with the flight PPTs. The forward port flight pressures compare similarly to both the analytically derived and wind-tunnel derived databases. Both databases match the aft port pressure flight data similarly above Mach 5, with the analytically derived database matching the flight data slightly better than the wind-tunnel derived database. The wind-tunnel derived database is a much better match to the aft pressure port flight data below Mach 5.

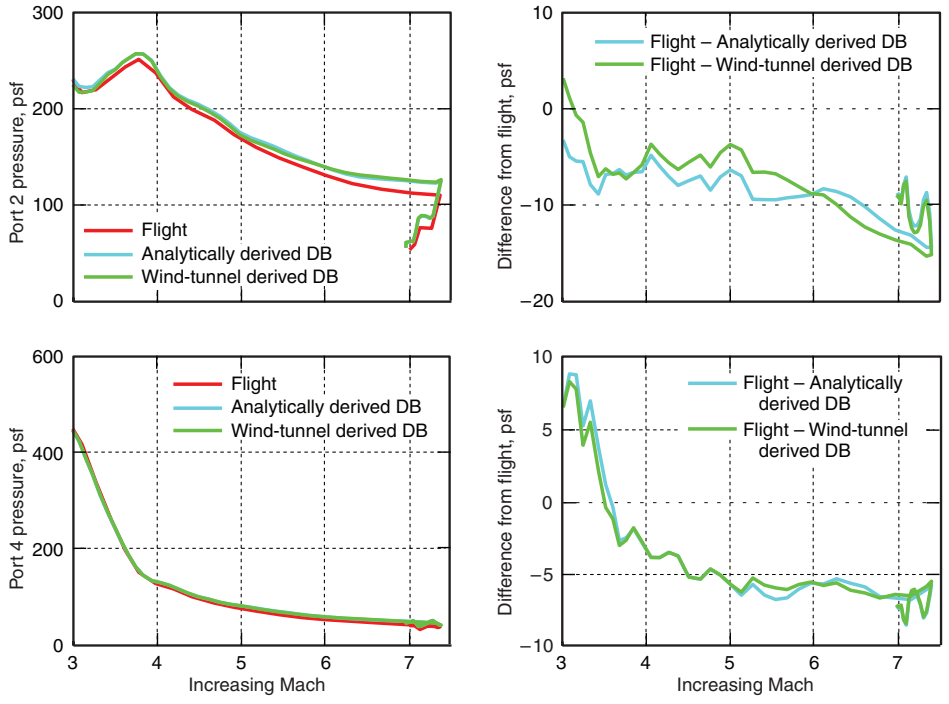

Fig. 11 Forward pressure port readings during the Mach 7 mission ascent.

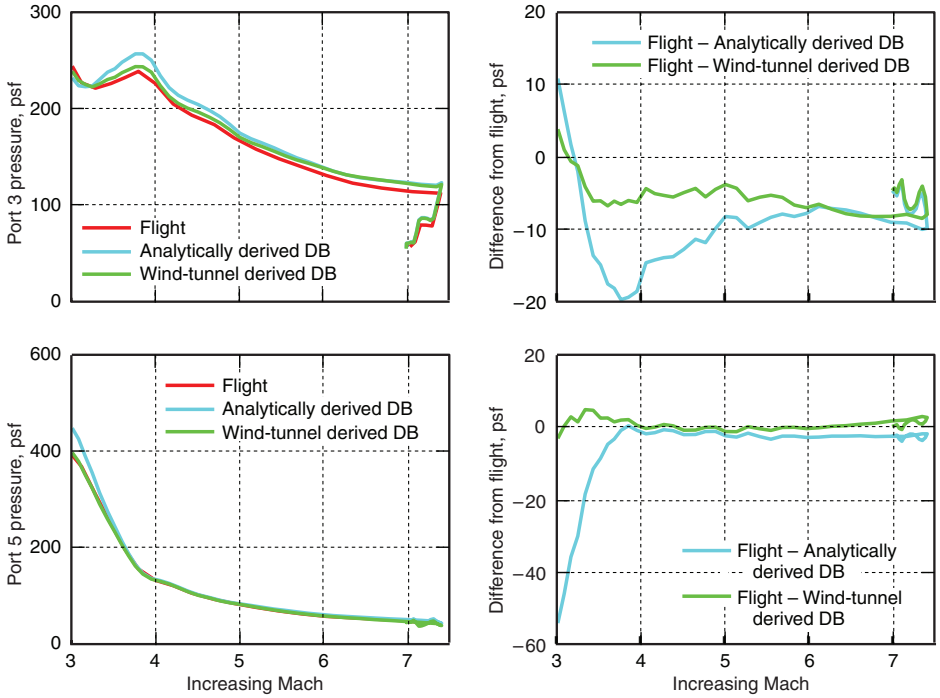

Fig. 12 Aft pressure port readings during the Mach 7 mission ascent.

X. Flush Airdata Sensing Angle-of-Attack Estimation from Flight Data

After the missions, flight data from the ascent and descent portions of each mission were run through the real-time flight algorithms to generate FADS α estimates. Two separate FADS α estimates were generated using calibrations derived from the analytically derived and wind-tunnel derived databases. The Mach number and dynamic pressure from the onboard INS were used as inputs to the algorithms. The onboard values were used to understand what the in-flight α estimates would have been with the two separate set of calibrations. This comparison was done to determine which of the two calibrations would have performed better in-flight. The FADS α estimates generated with the analytically derived database are hereafter referred to as the analytically derived α estimates, and the estimates generated with the wind-tunnel derived database are hereafter referred to as the wind-tunnel derived α estimates. The analytically derived database calibrations were used real-time onboard the X-43A during the two missions.

Figure 16 compares the inertial and BET α values from the descent portion of the Mach 7 mission to the analytically derived and wind-tunnel derived α estimates. The inertial α values are shown for comparison purposes because it is what the flight control laws normally use. During dynamic maneuvers such as the PID maneuvers, greater differences are seen between the FADS α estimate, BET α, and

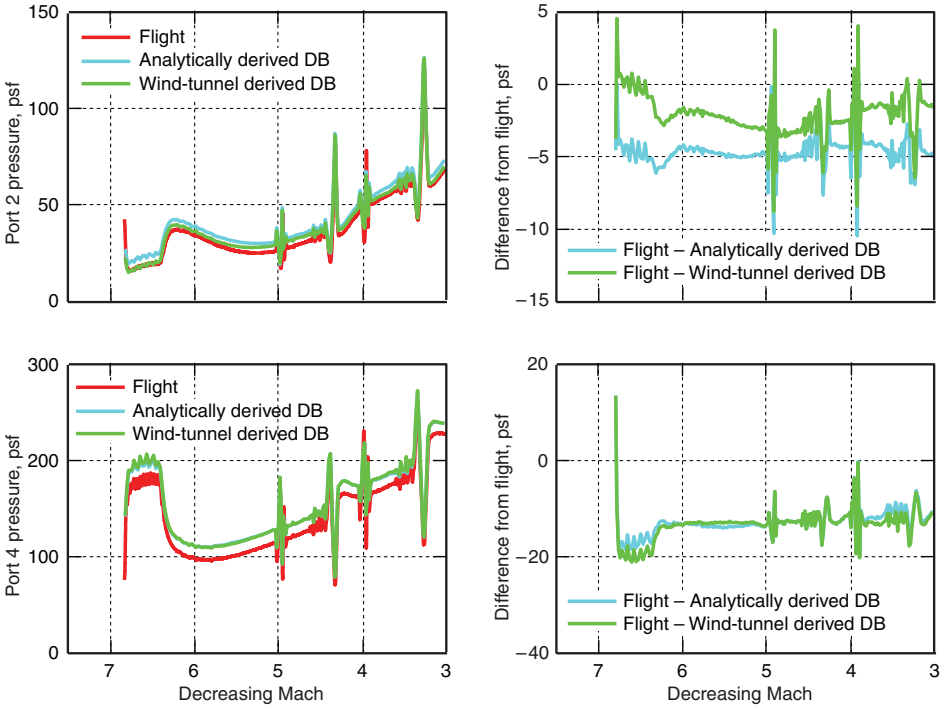

Fig. 13 Forward pressure port readings during the Mach 7 mission descent.

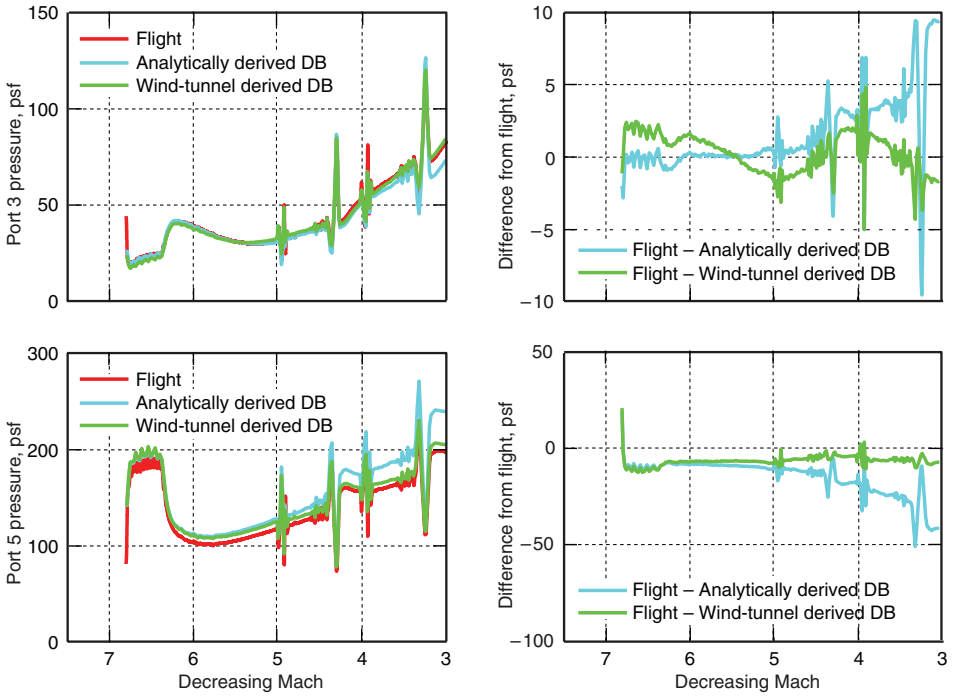

Fig. 14 Aft pressure port readings during the Mach 7 mission descent.

inertial α because the FADS α estimate lags the BET and inertial α values due to the FADS pneumatic system lags. The wind-tunnel derived α estimate tracks the BET and inertial α values to within 0.5 deg, which is significantly better than the analytically derived α estimate below Mach 5. When compared with the BET α estimate, the analytically derived calibrations are slightly better than the wind-tunnel derived calibrations above approximately Mach 6. Below Mach 5, the wind-tunnel derived calibrations result in a better α estimate as compared with the BET.

Figure 17 compares the FADS, inertial, and BET α estimates during the descent portion of the Mach 10 mission. The wind-tunnel derived FADS α estimates perform slightly worse than the analytically derived FADS α estimate above approximately Mach 6, and perform significantly better below this point. The wind-tunnel derived FADS α estimate is within 0.8 deg of the inertial and BET values at the higher Mach numbers, and even closer at the lower Mach numbers.

In the timeframe below Mach 5 for both missions, the wind-tunnel derived FADS α estimates match the BET α estimates better than the analytically derived FADS α estimate. This indicates that the wind-tunnel data matches the flight data better than theory below Mach 5. Above Mach 6, the analytically derived FADS α estimate matches the BET α estimate slightly better, indicating that theory matches the flight data better than the wind-tunnel results above Mach 6.

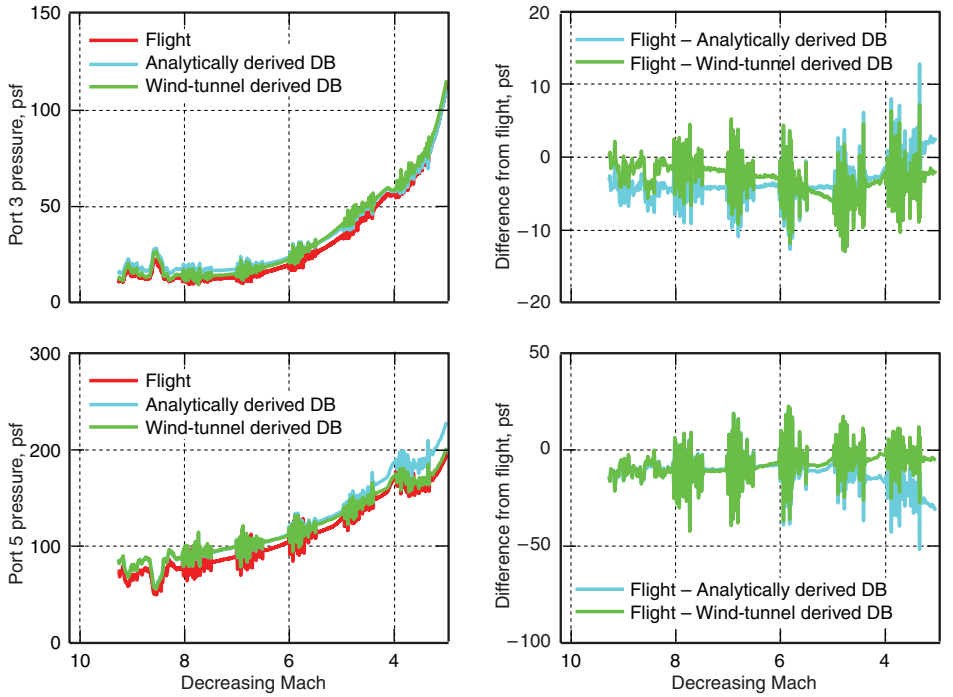

Fig. 15 Aft pressure port readings during the Mach 10 mission descent.

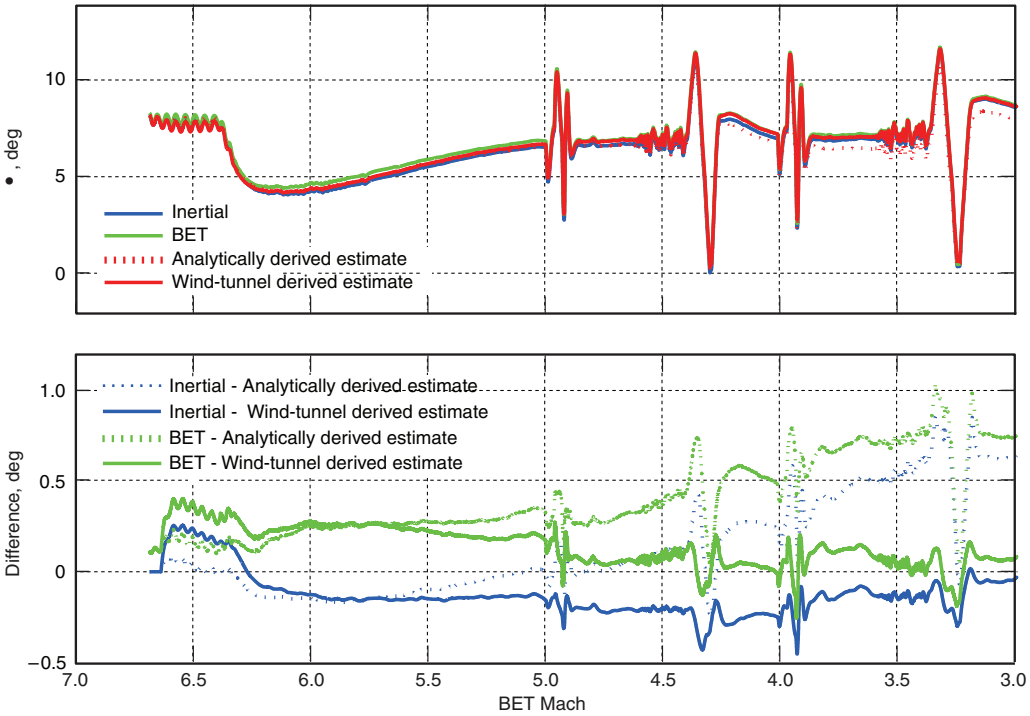

Fig. 16 FADS α comparisons using the theory and wind-tunnel derived databases for the Mach 7 mission descent.

XI. In-Flight Angle-of-Attack Estimation Algorithm Performance

The in-flight performance of the FADS α estimation algorithm is briefly discussed to demonstrate the viability and maturity of the algorithm. The analytically derived FADS calibration database was used in the real-time flight algorithms, because before the flights it was believed to provide the most accurate calibrations.

The FADS α real-time estimation algorithms were intended to provide an input to the X-43A flight control laws during the free-flight portion of the mission, which includes the descent portion following the scramjet engine test. Results are discussed in detail only for the descent portion of the missions, which is the designed operating region. Figure 18 compares the FADS α estimate for the Mach 7 mission with the onboard inertial and BET values. The inertial α value is shown because it is an input to the FADS algorithm and used to determine the validity of the FADS α estimate. Figure 18 also shows the differences between the FADS α estimate compared with the inertial and BET values, and includes the algorithm's bounds for determining FADS α estimate validity. Throughout the Mach 7 mission, the BET and onboard inertial α values are similar. The FADS α estimate remains within 1 deg, and usually much closer, of the inertial and BET values throughout most of the descent portion of

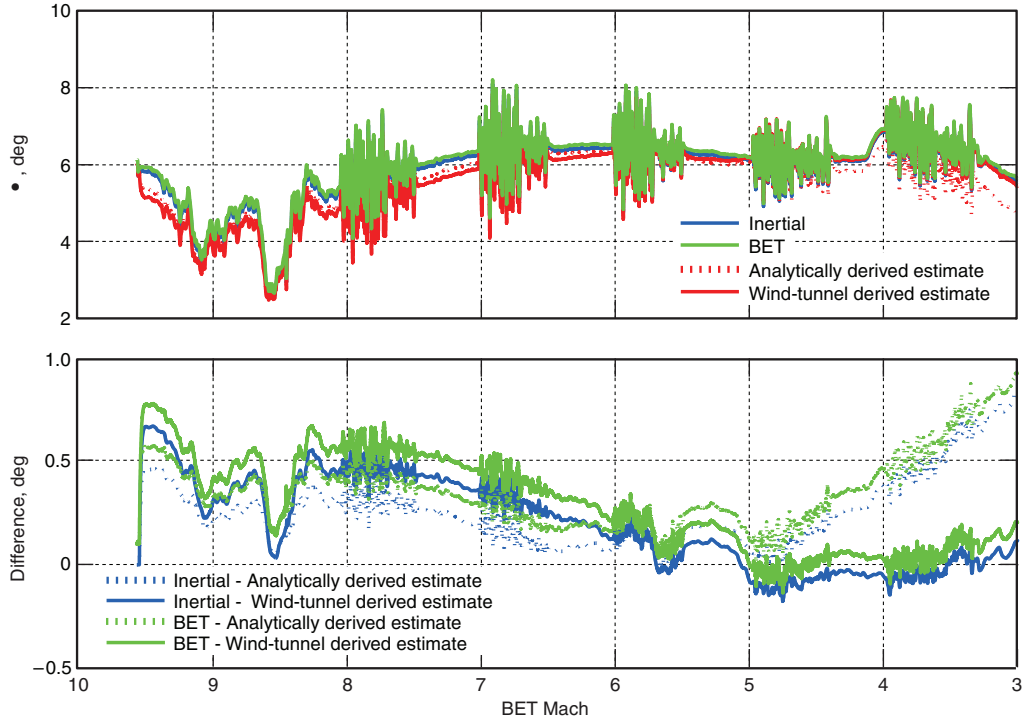

Fig. 17 FADS α comparisons using databases for the Mach 10 mission descent.

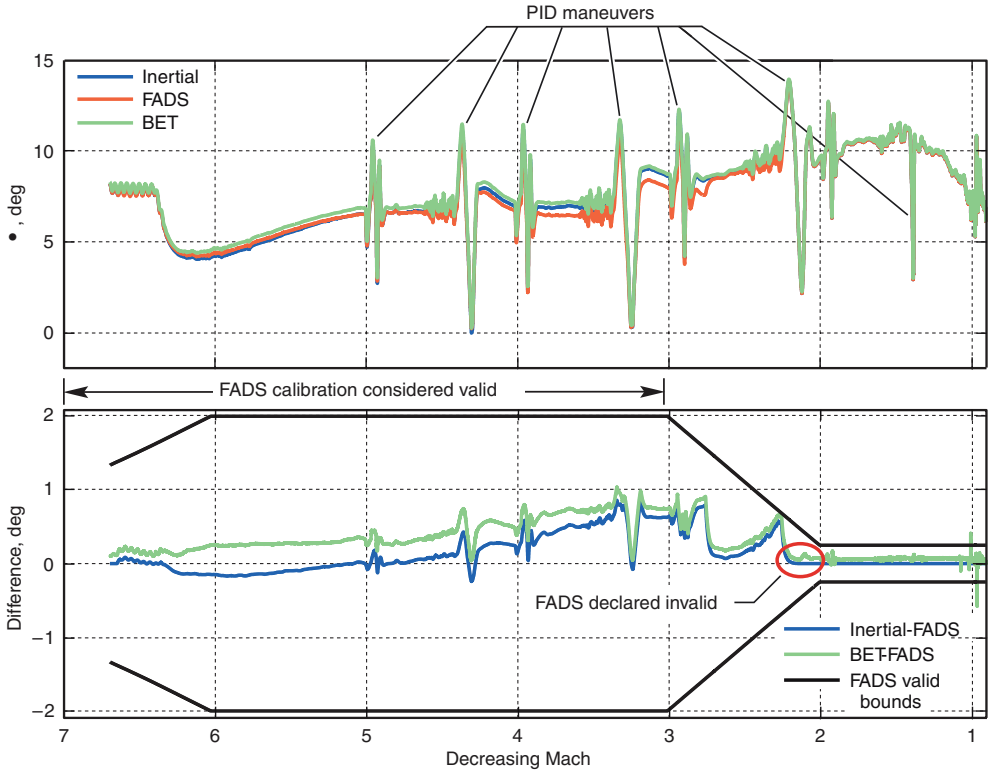

Fig. 18 Inertial, analytically derived FADS, and BET α comparisons for the Mach 7 mission.

the Mach 7 mission. At the higher Mach number, the FADS α estimate is within a few tenths of a degree of the inertial and BET values until the Mach 5 PID maneuver. After the Mach 5 PID maneuver, increasing differences are seen between the FADS α estimate, and the inertial and BET values. This increasing difference is due to the previously discussed differences seen in the analytically derived pressure port readings as compared with flight data. Following the Mach 3 PID maneuver, the difference between the FADS α estimate

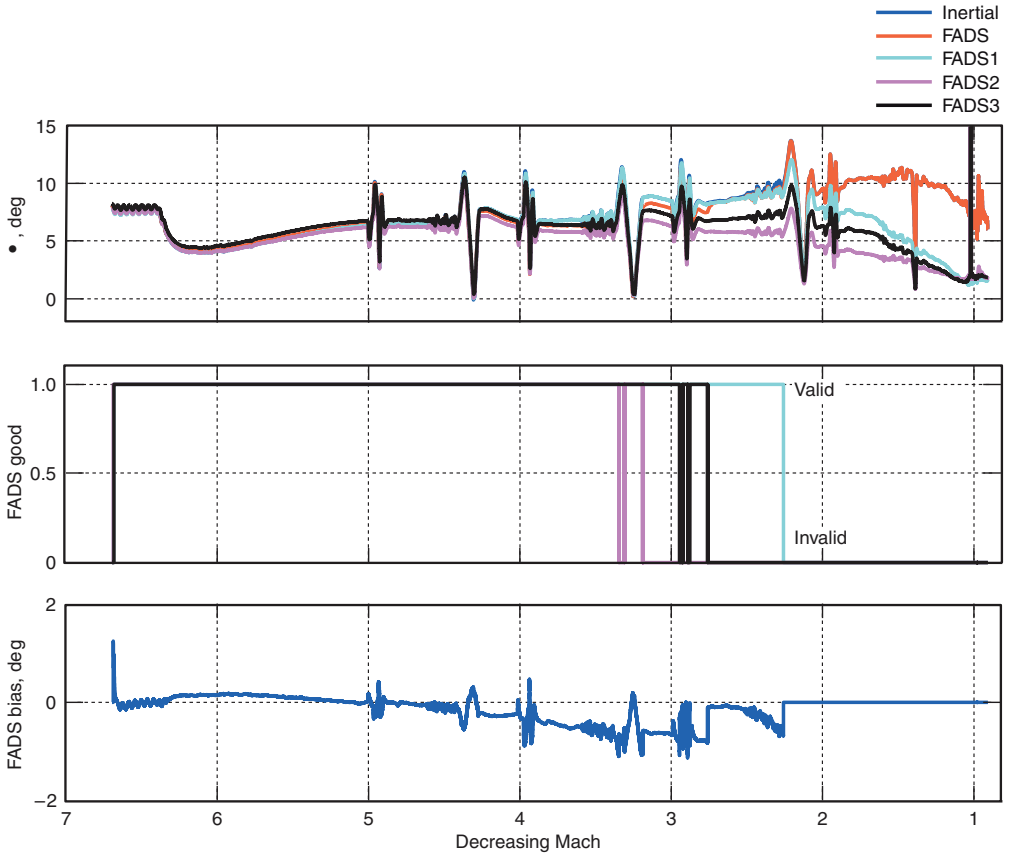

Fig. 19 Separate analytically derived FADS α estimates and FADS bias for the Mach 7 mission.

and the inertial α was outside of the allowable bounds, thus the FADS α estimate was declared invalid and only the inertial α was used by the flight controls until impact. Figure 18 highlights the time frame immediately after the FADS α estimate has been declared invalid. At this time the FADS α estimate is set to the same value as the inertial α value. There is a nonzero difference between the BET and FADS α because the BET α is based on trajectory reconstruction and does not exactly match the inertial α. The FADS valid bounds decrease following the Mach 3 PID maneuver as a means of intentionally failing the FADS α estimate as the Mach number decreased to a point beyond which the analytically derived FADS pressure predictions could not be compared with wind-tunnel data. During the Mach 3 PID maneuver, the FADS α estimate begins to better track the inertial and BET values for a short period of time. The reason for this better performance is that the FADS2 and FADS3 estimates are determined to be invalid, and FADS1 was used exclusively to calculate the FADS α estimate. Figure 19 shows the point at which FADS2 and FADS3 exceed their individual tolerances and are determined to be invalid.

Figure 19 shows the inertial α estimate (blue line) compared with the FADS α estimate (red line) and the three separate α estimates used to determine the FADS α estimate. The inertial and FADS α estimate values are very similar throughout the descent portion. After all of the FADS α estimates are considered invalid, the FADS α estimate is set to the inertial α value. Also shown in Fig. 19 are the FADS flags used to determine the validity of the three separate estimates, and the FADS bias that is applied to the inertial α to compute the FADS α estimate. The FADS1 α estimate, which uses the two forward ports (ports 2 and 4), tracks the inertial α better than the FADS2 and FADS3 estimates, both of which rely on port 5. The FADS1 α estimate is considered valid until nearly the end of the Mach 3 PID maneuver, and the FADS2 and FADS3 α estimates had drifted enough from the inertial value to be considered invalid around Mach 3. The FADS2 and FADS3 α estimates increasingly differ from the inertial and BET α values during the Mach 5 PID maneuver due to the port 5 pressure reading being lower than predicted by the analytically derived FADS pressure database.

As previously discussed, the inertial α value is passed through a Mach-dependant pneumatic lag model in the FADS α estimation algorithm before being compared with each FADS α estimate. Figure 20 compares the inertial and lagged inertial values with the FADS1 α estimate during the Mach 5 PID maneuver. The differences between the FADS1 α estimate, and the inertial and lagged inertial values are also shown. The FADS1 α estimate tracks the dynamics of the lagged inertial value within 0.5 deg during the PID maneuvers, which consist of rapid changes in α, and within 0.1 deg when α is not rapidly changing. The small differences between the dynamic component of the lagged INS α and FADS α estimates indicates the FADS pneumatic lag model accurately models the system pneumatic pressure lags. Results for the other two FADS α estimates are similar, indicating good pneumatic lag models.

The real-time FADS α estimation algorithm performed acceptably during the two missions. This performance demonstrates the feasibility of this algorithm for generating an air-mass-corrected α

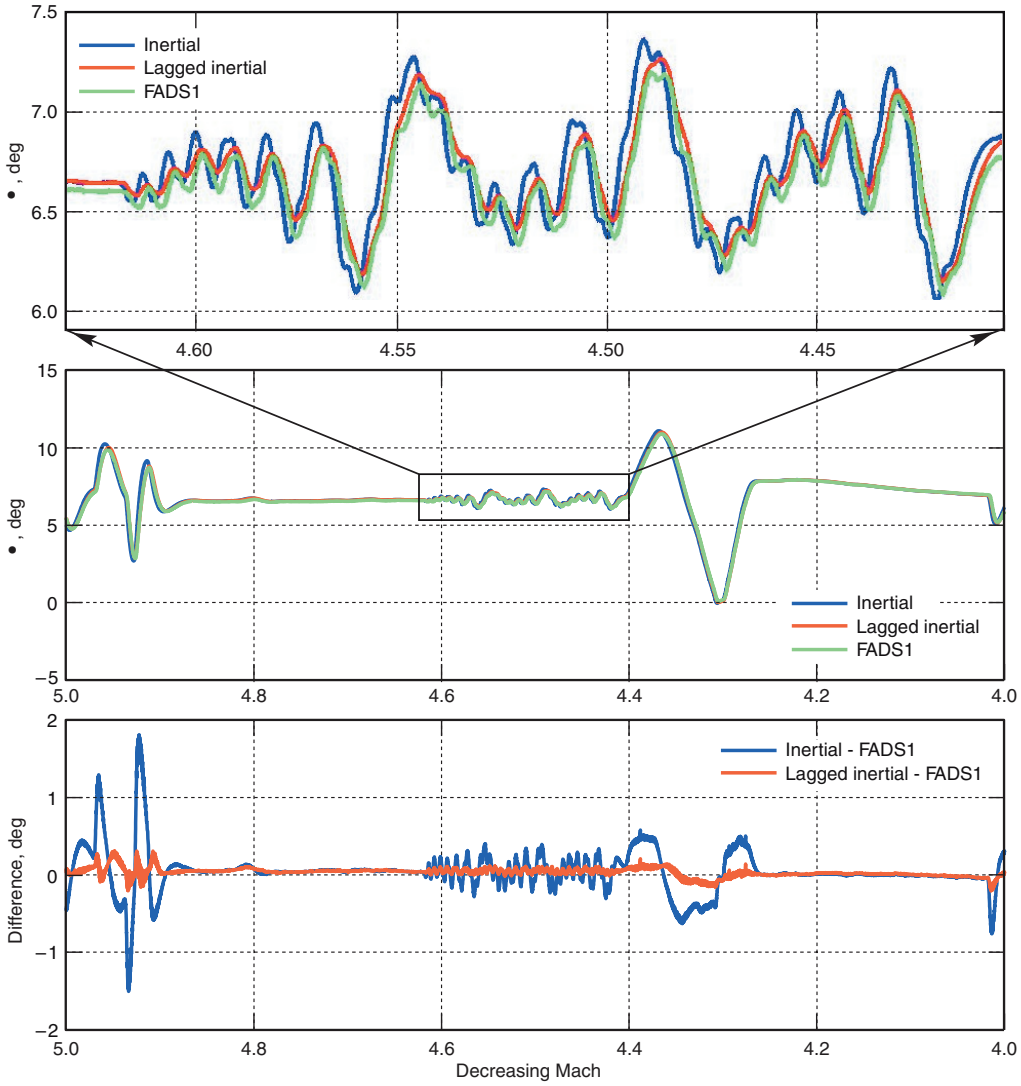

Fig. 20 Analytically derived FADS1 α estimate compared with inertial and lagged inertial α values for the Mach 7 mission during a portion of the Mach 5 PID maneuver.

estimate for a sharp-nosed hypersonic vehicle. The algorithm is only as good as the database from which the calibrations are derived. The in-flight performance of the FADS α estimation algorithm would have been better below Mach 5 if the calibrations had been derived from a database based on the wind-tunnel data. However, the analytically derived calibrations, which were used during the Mach 7 mission, provided an estimate of the α within 1 deg, and usually much better, of the best postflight estimate. This performance aided the flight control laws in guiding the vehicle to a successful descent during the Mach 7 mission.

XII. Conclusions

A flush airdata sensing system was flight-tested on the X-43A. Analytically derived and wind-tunnel derived pressure port databases were constructed for use in the FADS angle-of-attack (α) estimation algorithm. Comparisons between flight data, an analytically derived pressure database, and a wind-tunnel data derived pressure database were presented. These comparisons indicated that the wind-tunnel data matched the flight data significantly better below Mach 5 for the aft pressure ports. The analytically derived database matched the aft pressure port flight data above Mach 5 slightly better than the wind-tunnel data, indicating that theory is a better match to flight data in this regime than the collected wind-tunnel data. Flight data from the forward pressure ports matched the analytically derived database and the wind-tunnel derived database similarly. Real-time estimates of angle of attack were generated in-flight by the FADS α estimation algorithm using the analytically derived pressure database. The real-time algorithm tracked the best postflight estimate of α within 1 deg, and usually much better, during both the Mach 7 and Mach 10 missions with the FADS α estimate being used during the Mach 7 mission to aid the inertial estimate. The FADS system data collected during the flight test of the X-43A demonstrates the feasibility of estimating α on a sharp-nosed hypersonic vehicle.

References

[1] Davis, M. C., Pahle, J. W., White, J. T., Marshall, L. A., Mashburn, M. J., and Franks, R., "Development of a Flush Airdata Sensing System on a Sharp-Nosed Vehicle for Flight at Mach 3 to 8," NASA TM-2000-209017, 2000.

[2] Freeman, D. C., Jr., Reubush, D. E., McClinton, C. R., Rausch, V. L., and Crawford, J. L., "The NASA Hyper-X Program," NASA TM-1997-207243, 1997.

[3] Ferlemann, S. M., McClinton, C. R., Rock, K. E., and Voland, R. T., "Hyper-X Mach 7 Scramjet Design, Ground Test and Flight Results," AIAA Paper 2005-3322, 2005.

[4] X-43A Mishap Investigation Board, "Report of Findings X-43A Mishap," Vol. 1, May 2003.

[5] Marshall, L. A., Corpening, G. P., and Sherrill, R., "A Chief Engineer's View of the NASA X-43A Scramjet Flight Test," AIAA Paper 2005-3332, May 2005.

[6] Marshall, L. A., Bahm, C., Corpening, G. P., and Sherrill, R., "Overview With Results and Lessons Learned of the X-43A Mach 10 Flight," AIAA Paper 2005-3336, May 2005.

[7] Bahm, C., Baumann, E., Martin, J., Bose, D., Beck, R. E., and Strovers, B., "The X-43A Hyper-X Mach 7 Flight 2 Guidance, Navigation, and Control Overview and Flight Test Results," AIAA Paper 2005-3275, May 2005.

[8] Baumann, E., Bahm, C., Strovers, B., and Beck, R., "The X-43A Mach 10 Mission Guidance and Control Updates, Rationale, and Flight Test Results," NASA TM-2007-214610, Jan. 2007.

[9] Ohlhorst, C. W., Glass, D. E., Bruce, W. E., Lindell, M. C., Vaughn, W. L., Smith, R. W., Dirling, R. B., Jr., Hogenson, P. A., Nichols, J. M., Risner, N. W., Thompson, D. R., Kowbel, W., Sullivan, B. J., Koenig, J. R., and Cuneo, J. C., "Development of X-43A Mach 10 Leading Edges," IAC Paper 05-D2.5.06, Oct. 2005.

[10] Karlgaard, C. D., Martin, J. G., Tartabini, P. V., and Thornblom, M. N., "Hyper-X Mach 10 Trajectory Reconstruction," AIAA Paper 2005-5920, Aug. 2005.

[11] Morelli, E. A., Derry, S. D., and Smith, M. S., "Aerodynamic Parameter Estimation for the X-43A (Hyper-X) from Flight Data," AIAA Paper 2005-5921, Aug. 2005.

[12] Baumann, E. A., "Tailored Excitation for Frequency Response Measurement Applied to the X-43A Flight Vehicle," NASA TM-2007-214609, Jan. 2007.

[13] Anderson, J. D., Jr., *Hypersonic and High Temperature Gas Dynamics*, McGraw–Hill, New York, 1989.

[14] Whitmore, S. A., "Development of a Pneumatic High-Angle-of-Attack Flush Airdata Sensing System," Society of Automotive Engineers Paper 912142, Sept. 1991.

[15] Whitmore, S. A., and Moes, T. R., "Failure Detection and Fault Management Techniques for a Pneumatic High-Angle-of-Attack Flush Airdata Sensing (HI-FADS) System," NASA TM-4335, Jan. 1992.

[16] White, J. T., "Results of the HYPER-X Research Vehicle (HXRV) Flush Air Data Sensing (FADS) System Wind Tunnel Test (AEDC VA435)," Hyper-X Rept. HX-DFRC-0308, Dec. 2003.

[17] Karlgaard, C. D., Tartabini, P. V., Blanchard, R. C., Kirsch, M., and Toniolo, M. D., "Hyper-X Post-Flight-Trajectory Reconstruction," *Journal of Spacecraft and Rockets*, Vol. 43, No. 1, Jan.–Feb. 2006, pp. 105–115.
doi:10.2514/1.12733

M. Miller
Associate Editor